Nanoindentation Hardness of Particles Used in Magnetorheological Finishing (MRF)

Introduction

Classical finishing processes of optics employ precisely shaped, viscoelastic pitch or polyurethane foam–faced tools to transfer pressure and velocity through an abrasive slurry to the workpiece. Material is removed by chemical and mechanical interactions among the abrasive (typically micron- to submicron-size cerium oxide or aluminum oxide), the carrier fluid (water), and the workpiece. Magnetorheological finishing (MRF)—a new method of polishing optics—is being studied at the Center for Optics Manufacturing (COM) at the University of Rochester. This method utilizes a suspension consisting of magnetic particles [typically carbonyl iron (CI)], nonmagnetic abrasive particles, water, and stabilizing agents. Figure 82.59 shows an MR polishing machine. Rotation of the bottom wheel takes the fluid from the delivery nozzle and drives it underneath the part, where there is a strong magnetic field. Under the influence of the magnetic field, the fluid behaves like a "plastic" fluid; it is the shear stress caused by the hydrodynamic flow between the part and the rotating wheel that removes the material.[1]

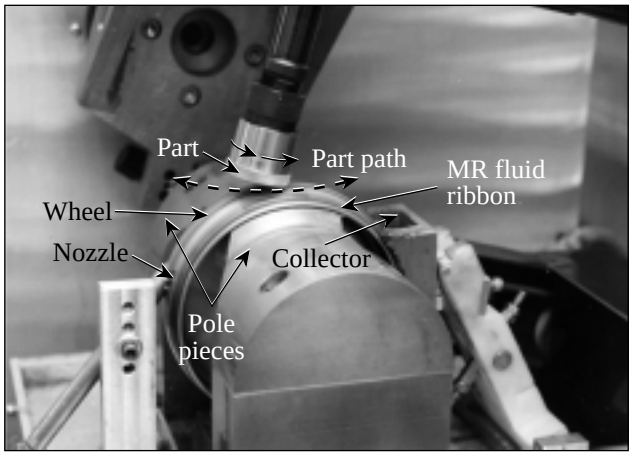

G4973

Figure 82.59
Photograph of the MRF polishing process. The fluid emerges from the nozzle on the left and is carried to the right into the polishing zone under the part surface by the rotation of the wheel. The pole pieces are part of the electromagnet that provides the magnetic field that stiffens the fluid into a ribbon.

Figure 82.60 shows an example of microroughness on the surface of an initially pitch-polished fused-silica part processed without part rotation and with a nonaqueous MR fluid. With all chemistry eliminated, what remains are parallel grooves approximately 16-nm peak-to-valley and 1-nm rms,[2] caused by microscratching along the direction of flow. The water in aqueous MR fluids "turns on" chemistry, and removal rates increase substantially. Removal rates increase further in aqueous-based MR fluids containing nonmagnetic polishing abrasives (e.g., Al_2O_3, CeO_2, and nanodiamonds).[3] The features of the grooves look similar to the ones shown in Fig. 82.60. It is not known whether it is the abrasive action of the magnetic or nonmagnetic particles, or a chemical contribution from water and the presence of the nonmagnetic particles that plays the most important role in enhancing removal. Nanohardness tests described here allow us to begin to understand more fully the role of the various magnetic and nonmagnetic abrasives in the removal process.

Many authors (see Ref. 4 for example) describe a hydrated layer at the glass surface caused by the chemistry of the aqueous slurry. This soft hydrated layer affects polishing since it is easier to remove than the bulk material. An abrasive that is softer than the bulk material could conceivably remove material from a hydrated layer, but a harder particle (under the same load) could penetrate farther into the layer and thus remove more material. Kaller[5] discusses both the importance of finding the unknown hardness of abrasive particles and how the abrasive should actually be softer than the material being polished. An interesting experiment would be to compare removal characteristics of particles of different hardness in the same chemical environments. The variation in groove depth as a function of particle hardness would estimate the extent of the hydrated layer. For this experiment to be of the greatest utility the actual hardness of the particle must be known. The work described above is in progress.[6] To support this work, particle-nanohardness measurements are reported here and compared to some materials important to optics.

The hardness of a material is typically measured by pushing a hard material into a softer one and measuring the area of residual deformation left on the softer material. The hardness is the indenting load divided by the area of the residual deformation. In the past, Steinitz[7] determined particle microhardness through microindentation (material hardness found through microindentation will be referred to as microhardness, and that found through nanoindentation will be referred to as nanohardness). His figures show that the particle areas being indented were of the order of 100 μm in size and that the size of an indent was about 20 μm. Loads from 25 to 300 g (about 0.25 to 3 N) were used. The author points out that relatively large loads were needed for these indents so that the diagonals could be accurately measured for the microhardness calculation. This limited Steinitz to relatively large particles. The particles that we are concerned with have a median diameter of about 5 μm, although it is possible to screen out ≈ 20-μm particles for study. The indent should therefore be significantly smaller than 20 μm for reasons that will be discussed later. These particles are still too small to be tested with a traditional microhardness tester. Small particles could be sintered or pressed together for ease of indentation, but heating or stressing the particles could change their mechanical properties.[7] Using the nanoindentation techniques described below, we are able to make smaller indents on much smaller particles than was done previously with microindentation, without altering the mechanical properties of the particles.

Nanoindenter

Hardness is measured with a commercially available nanoindenter.[8] The indenter is a Berkovich three-sided, pyramidal diamond that accommodates maximum loads up to about 700 mN. Our experiments used maximum loads of 1 and 5 mN. This instrument applies a load by magnetic coil; the displacement of the indenter is continuously measured with a capacitance gauge. The displacement can be measured to within ±0.04 nm and the output voltage from the loading operation to within 4 μV. The loads and displacements for our experiments are such that the measurement error is much less than 1%.

The nanoindenter's computer-automated system allows the user to choose the indentation experiment (loading rate, maximum load, drift correction, etc.) and location of the indent, leaving the instrument unattended as the experiment is performed. A typical experiment takes only about 15 min, but the time depends on the environment where the nanoindenter is located and the number of indents made. The first part of a test requires that the instrument settle to a user-specified critical drift rate. The indenter is kept in an insulated cabinet on a vibration isolation table. If the room containing the instrument has significant vibrations or temperature gradients, it may take some time for the drift rate to settle to the user-selected value. Our tests utilize the default critical drift rate of 0.05 nm/s.

Both nanohardness and the elastic modulus can be calculated via the load-displacement curves.[9] Since the load-displacement curve is of greatest interest, it is important that the particle be constrained from displacing due to the indenter loading from the top. That is, the measured displacement must be due to the motion of the indenter into the particle surface, and not due to the motion of the particle. For this reason,

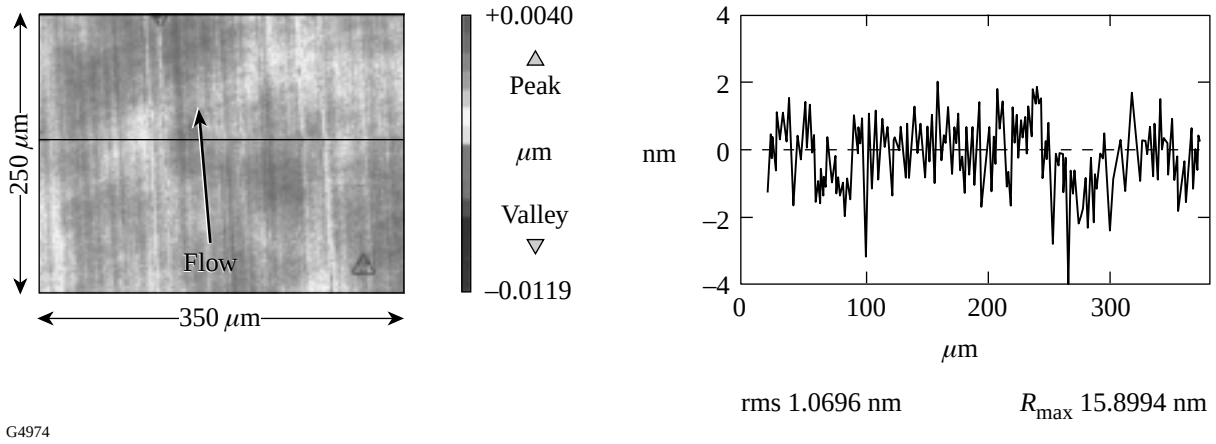

Figure 82.60
Microroughness on the surface of a fused-silica part after MRF without rotation. The MR fluid contains CI and nanodiamonds in a nonaqueous carrier fluid. The grooves are parallel to flow and are a result of particle/glass interaction.

magnetic particles are fixed rigidly to a glass substrate by embedding them in an epoxy matrix, and nonmagnetic particles are cast in a polymer substrate (phenol-formaldehyde or Bakelite). There is evidence in the literature that the substrate affects the measured properties of thin films.[10,11] Initial screening experiments before this study suggested that this problem influenced small-particle indentation as well. Special sample preparation techniques described below were devised to avoid this effect.

One of the strengths of the nanoindenter is that it allows precise positioning of indents. This ability allows us to search for and indent individual particles. Indents can be positioned to within 0.4 μm, but this accuracy is reduced by thermal drift and the accumulation of small errors.[8] Frequent system calibration allows for the precision necessary to indent 5-μm particles, but there are fewer failed tests (i.e., no particles indented) if the indented surface is approximately 20 μm in diameter. The larger particle size reduces the importance of any positioning error caused by the nanoindenter translation stages. For this reason, the particles are suspended in methanol and passed through a sieve[12] to separate out larger particles for testing. A second option, if the particles are relatively small, is to create an array of indents near a particle. For example, a line of indents can be defined so that, while some of the indents will be into the epoxy, the rest will be on the particle. Results reported here are from experiments performed by either method.

Sample Preparation for Magnetic Particles

The magnetic particles (primarily CI) are processed as illustrated in Fig. 82.61. After they are sieved, the particles are placed on a BK7[13] glass substrate, which is set on top of a rare earth permanent magnet.[14] The roughness of the substrate is about 1 μm rms or smoother, and the substrate is flat to within about 1 to 10 μm per cm^2 of surface. These specifications are not critical, but height variations in the substrate surface of the order of tens of microns per centimeter are avoided. Next, a two-part, room-temperature curing epoxy[15] is spread onto a polymer foil,[16] and the foil is placed over the particles, epoxy side down. A microscope slide is placed on top of the back side of the polymer foil (the foil prevents the epoxy from adhering to the slide), and finally a mild iron weight (40 g) is placed over the slide [see Fig. 82.61(a)]. Since the iron weight is attracted to the magnet, the epoxy/particle matrix is forced into a thin layer, and the microscope slide helps to create a more uniform surface on the epoxy. Figure 82.61(b) shows how the epoxy is believed to surround the CI particles to hold them in position during curing.

This fabrication procedure accomplishes two things: First, the particles are attracted downward to the magnet. This pulls the bottom particle layer toward the BK7 surface. Second, when placed in a magnetic field, the magnetic particles tend to align into chain structures.[17] This helps prevent epoxy from getting in between adjacent particles. The perceived advantage is that by having chains of particles resting against the glass substrate, we minimize the possibility of measuring a reduced hardness due to effects of a compliant substrate mentioned above.[10,11] The assembly shown in Fig. 82.61(a) is left to cure in air for 24 h. Once the epoxy has cured, the mild iron weight and microscope slide are removed from the magnet. The polymer foil is stripped away, leaving the BK7 substrate and CI/epoxy matrix. The matrix surface is ground by hand on a serrated, cast iron lap with 9 μm alumina[18] to thin the film and create flat surfaces on the particles. Grinding is performed as described by Parks *et al.*[19] so that work hardening of the particles is minimized. A load of about 35 kPa (about 5 psi)[20] is used with the iron lap rotating at 35 rpm. This step takes no more than a few minutes. The grinding step always results in some wedge being put into the surface, leaving an epoxy/CI

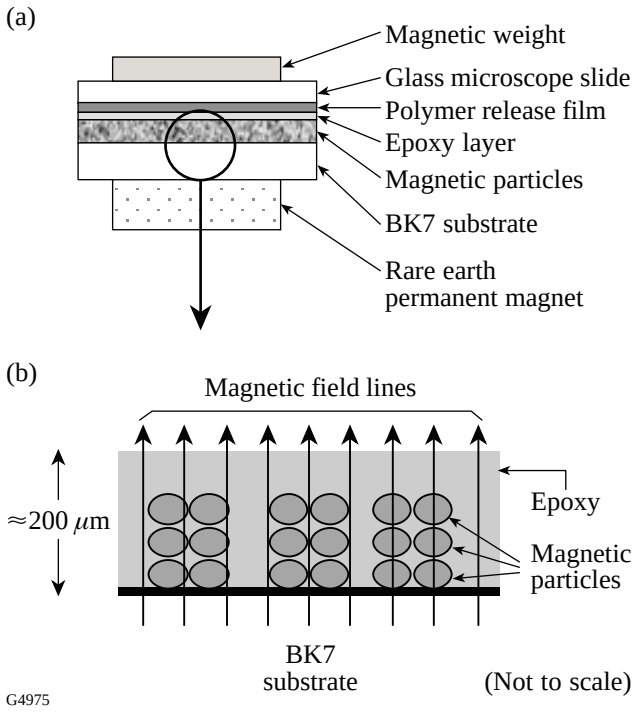

Figure 82.61
(a) Schematic diagram of the method used in sample preparation. The particles and epoxy are sandwiched between two hard, flat surfaces so that a thin layer is formed. (b) Sketch of how the particles are thought to orient in the epoxy layer shown in (a) under the influence of a magnetic field.

film that decreases in height from one side to the other (see Fig. 82.62). The grinding step is complete when the glass substrate starts to become visible. In this way, we know that there is a thin layer of the composite film where indents can be taken very near the glass substrate.

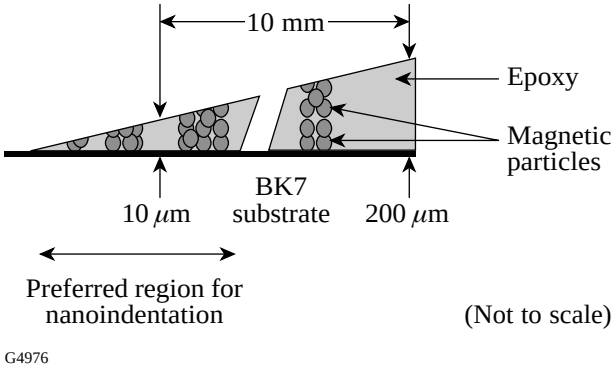

Figure 82.62
Schematic diagram of the sample after the magnet has been removed and the top layer of epoxy has been ground and polished away. The flats on the particles constitute the potential indent sites.

Samples are polished with light pressure on a cerium oxide impregnated felt lap[21] at a rotation speed of 50 rpm. This step is monitored with the help of an optical microscope.[22] The polishing phase is considered complete when few polishing grooves can be seen on the CI surfaces at 1000× magnification. This step is a manual operation that takes approximately 30 min, depending on the skill of the operator.

At the conclusion of sample preparation, the CI/epoxy film thickness varies from about 200 μm down to zero (at the glass surface) over a distance of about 10 mm as measured by mechanical profilometry.[23] Indents are placed where the film is about 25 to 50 μm thick. As shown schematically in Fig. 82.62, the goal of our sample preparation process is to create polished flats on the CI particles.

Sample Preparation for Nonmagnetic Abrasive Particles

The above technique for sample preparation is appropriate only for magnetic particles since we take advantage of the magnetic attraction of the particles to try to minimize the effect of deformation of the embedding medium. The nonmagnetic particles are treated differently. They are mixed with Bakelite pellets in a ratio of about 1 to 5. This mixture is then put into a 1.25-in.-diam cylindrical mold, placed into a press,[24] heated to 150°C, and pressed under 5000-psi pressure. It is assumed that this heat and pressure do not change the particle properties. The heat and pressure allow the Bakelite to form a network around the abrasives so that they are held in place during indentation experiments. The Bakelite sample is then ground and polished as described above until several particles are exposed. We have found that the Bakelite medium has a hardness and elastic modulus of about 0.4 GPa and 7 GPa, respectively. These values are significantly lower than those of the particles being tested, so deformation of the embedding medium is a concern (discussed below).

Validation of Tests

It is important to have a way to verify that indentations are actually being placed on an individual particle. Figures 82.63(a) and 82.63(b) show SEM[25] images of a carbonyl iron particle surface after indentation testing. The programmed maximum load was 5 mN. The test was set up to put an initial indent in the center of the particle and follow it with four more indents spaced 2 μm apart. The five indents are clearly shown in Fig. 82.63(a). Figure 82.63(b) shows a close-up view of two of the indents. The sharpness and repeatability in size of the indents are apparent. Indenter tip radius is 20–80 nm[8].

The sample thickness should be four to ten times larger than the depth of an indent.[10] Also, indents should be more than two times the size of any "stress deformation" that results from indentation. This prevents deformation due to neighboring indents from interacting.[26] Since most indents are approximately 200 nm deep, particles greater than 2 μm in size are sufficiently large for these loads. We choose relatively large particles and avoid the edges of particles so that we meet this criteria. The indents in Fig.82.63 are for illustration only. Quantitative data are obtained mostly by placing a single indent on a single particle. It should be noted, however, that the nanohardness values obtained from the indents shown in Fig. 82.63 were consistent with nanohardness values obtained from other tests performed on the same particle type.

If the particles are particularly small, it might be advantageous to make arrays of indents. In this case, care must be taken to identify valid indents from invalid ones. Figure 82.64 shows the indenter load/displacement curves of three indents from a linear array (similar to Fig. 82.63) on a single CI particle. The maximum load was 5 mN for all three indents, but the vertical displacement of the indenter was about 220 nm for indent 1, about 300 nm for indent 2, and about 550 nm for indent 3. The projected area and calculated nanohardness varied accordingly. The nanohardness was 715 kgf/mm^2 (7.01 GPa) for indent 1, 370 kgf/mm^2 (3.63 GPa) for indent 2, and 86 kgf/mm^2 (0.84 GPa) for indent 3. This wide range in the

measured nanohardness indicates that there is some error in the measurement.

The reason for the variation in the nanohardness for this single particle is evident from the three load/displacement curves in Fig. 82.64. The first indent shows typical loading and unloading behavior[9] for a single, hard material, whereas the second and third indents show a clear slope change in the loading curve (circled in Fig. 82.64). It is believed that this slope change is due to epoxy contamination around the edge of the particle. For the second and third indents, as the load is applied, the indenter first encounters an epoxy film, and the shallow slope of the loading curve is due to the fact that the epoxy is much softer than the CI. The change in slope of the loading curve can be explained by the fact that the thin material under load becomes more stiff (the slope of the curve increases) as the indenter is influenced by the underlying material. That is, we expect the slope of the loading curve to increase due to both elastic and permanent deformation as the indenter moves through the epoxy layer. Hay and Pharr[11] use a similar method to monitor the effects of a thin, hard film on a soft substrate. In their work, the slope of the loading curve becomes shallower as the soft substrate begins to flow under the hard film. As expected, the loading curve becomes steeper in our case since we have a thin film of soft material on a hard substrate. Such an interpretation is also consistent with a quantitative estimate of contact zone width based on the Sneddon solution of a rigid cone indenting an elastic half-space of a material with the properties of epoxy.[27] For these reasons indent 1 would be considered a successful indent, whereas indents 2 and 3 would not.

Krell *et al*.[28] discuss another consideration for indentation experiments. It is possible that a particle could be pushed into the embedding medium under the influence of the indenting load. By creating chains during sample preparation of magnetic particles and indenting particles near the BK7 surface, we minimize the chance of particle motion. The nonmagnetic particles are simply sitting in a relatively soft Bakelite matrix. It is conceivable that a small particle could be pushed into the matrix by the indenting load. To estimate this effect, consider

(a)

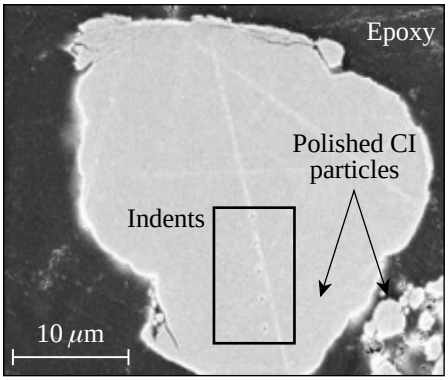

(b)

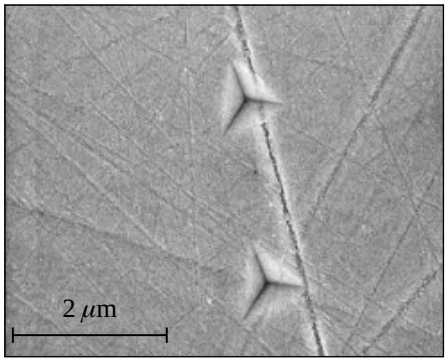

G4977

Figure 82.63
SEM of a large CI particle after a set of five indentations at 5-mN maximum load. The initial indent was placed in the middle of the particle, and the five indents were spaced 2 μm apart. This demonstrates the ability of the nanoindenter to place multiple indents precisely on a 20- to 25-μm-diam particle. Photographs like these are very difficult to obtain because of the difficulty in locating the indentation site after moving the sample from the nanoindenter to the SEM.

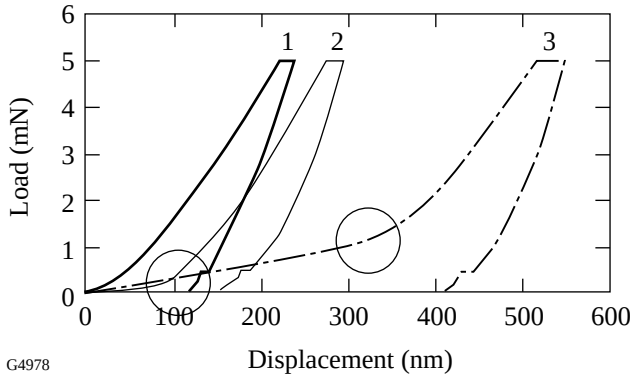

G4978

Figure 82.64
Load/displacement curves of three indents placed in a linear array on a single particle. The continuous behavior of indent 1 suggests a legitimate particle indent, whereas the slope changes in indents 2 and 3 (shown circled) suggest that there may be a region on the edge of the particle contaminated by the epoxy. Indent 2 shows a small region at the beginning of the loading, suggesting a small soft layer between the indenter and the particle. Indent 3 has a much larger region with this shallow slope, suggesting a deeper soft layer. Indents with these distinct changes in slope are not used.

the particle shown in Fig. 82.63(a). The area of this particle is approximately 30 μm × 30 μm (900×10^{-12} m^2) and subject to a 5-mN load. The approximate stress underneath the particle is the force divided by the cross-sectional area or 5.6 MPa in this case. This is two orders of magnitude below the hardness of the Bakelite or epoxy matrix. As the particle size decreases, the applied stress approaches the hardness of the matrix material. For this reason, low indenting loads are used, and particles on the large end of the size distribution are tested.

Finally, a problem that may affect both magnetic and nonmagnetic particles is the indentation-size effect (ISE). Lambropoulos *et al.*[29] and Fang[30] discuss this phenomenon in microindentation tests where the microhardness is a function of the applied load (and therefore size) of the indent. More recently Sangwal *et al.*[31] used an atomic force microscope to study ISE in nanoindentation experiments. Specifically, they report that the nanohardness decreases with an increase in indentation size and that there is a large discrepancy between hardness due to nanoindentation and microindentation of MgO.

Dahmani *et al.*[32] show that the elastic modulus and nanohardness of fused silica measured with nanoindentation agree with published results (the nanohardness was compared with a Vickers microhardness test[33]). This means that the low loads used in nanoindentation are not an immediate cause of ISE. We have also performed experiments at both 1-mN maximum load and 5-mN maximum load. A different nanohardness measured at the two different loads would be a sign that either ISE is a problem and/or the particle was moving relative to the indenter. None of our experiments showed a difference at the two loads, so these effects are not considered significant for our experiments. Sangwal *et al.*[31] perform indents at a load of 10 μN, which is two orders of magnitude below the load that we use. Also, they mention that their indentations fully recover after a sufficiently long time. Our indents do not recover. The fact that we are able to take SEM scans of indents a week after indentation tests is evidence of permanent deformation of the material. It is believed that their low loads and evidence of complete indent recovery put them in a different experimental regime.

Prior Work

Previously obtained hardness data for materials of interest to optics fabrication have typically been measured using either a Moh's test[34] or microindentation techniques on bulk or sintered samples. The Moh's scale is derived from a scratch test that uses ten minerals of increasing hardness. A substrate material is assigned a number on the Moh's scale according to the hardest standard mineral for which there is a visible scratch during a simple abrasion operation.[34] This is a qualitative test, but it gives relative hardness values for different substrate materials against known standards. Microindentation is a more quantitative experimental technique that typically uses a four-sided, pyramidal indenter (usually a Knoop or Vickers diamond) to permanently deform a material under a known load (1 to 1000 gf). The hardness of a material is the applied load divided by a measure of the area of the indent.[26] The Vickers and Knoop microhardness numbers are similar in magnitude.[35] More recently, it has been suggested that the hardness of submicrometer particles may be estimated by associating the hardness to the density of the material.[36] This correlation is unknown and is complicated by internal porosity of the particles. Results reported here for CI show the hardness–density correlation to be invalid.

This is the first work that has utilized nanoindentation to determine the hardness of small abrasive particles. Dahmani *et al.*[32] show that the Berkovich indenter measures a nanohardness similar in value to that from a Vickers microindent. Therefore we validate our results using existing microhardness data from bulk materials to compare with nanohardness results. Moh's data is used for comparison where no microhardness data exist in the literature.

1. Hard and Soft CI

The magnetic particles of interest to us are the "hard" and "soft" carbonyl iron particles that are typically used to prepare aqueous suspensions of MRF. These powders are formed from the decomposition of liquid iron pentacarbonyl. This process is explained elsewhere.[37–39] The high microhardness of the hard CI particles is attributed to the presence of carbon, oxygen, and nitrogen[37] and/or high internal stress in the material,[39] but does not appear to be clearly understood. Pfeil[37] cites a Vickers microhardness (25-g load) of about 850 kgf/mm^2 (8.33 GPa) for the hard carbonyl iron particles. Softening is achieved by annealing in a hydrogen environment to drive out the carbon, oxygen and nitrogen impurities. Boehm[40] discusses this annealing process and claims that, initially, the microhardness rises with heat treatment. Eventually it drops when the temperature is raised above 500°C. Boehm confirms Pfeil's result for the hard CI and gives a minimum microhardness of 280 kgf/mm^2 (2.75 GPa) for the softer, reduced CI. Finally, Ebenhoech[38] cites a Vickers microhardness of 900 kgf/mm^2 (8.82 GPa) for the hard CI and 100 kgf/mm^2 (1 GPa) for the soft CI at the same 25-g load. No details about the tests are given.

2. Nonmagnetic Abrasives

Six nonmagnetic particles have also been chosen for nanohardness tests since they are often used in grinding and polishing. Two types each of alumina and cerium oxide were chosen since they are of particular interest to optics fabrication. The two types of alumina differ in that one is used for grinding and one for polishing. The cerium oxide samples are both refined from a common ore, but with different heat treatments. We also tested silicon carbide and cubic zirconia particles, which were chosen because (1) they, too, are commonly used in optical fabrication and (2) the existing microhardness data in the literature helps to further verify our test results.

Microindentation hardness data for nonmagnetic abrasives exist in the literature. Krell *et al.*[28] test various alumina abrasives and discuss how the particle hardness and fracture toughness can affect the grinding efficiency. They also discuss the importance of knowing the hardness of individual abrasive particles as opposed to bulk values, especially in sintered specimens. Their experiments utilize 0.6-mm-mean-sized samples embedded in an epoxy matrix. They use Vickers indents at 10-N load. They also discuss the effect of the substrate and magnitude of the load on their measurements. Namely, if they use a higher load, the particles are pushed into the matrix. If they use a lower load, then they have difficulty measuring the size of the indent. We discussed the problems associated with using a high load, but we do not have their problem associated with low loads since our hardness is determined from the load/displacement curve. Our loads are four orders of magnitude less than theirs, which allow us to measure smaller particles in more-localized regions. Their results for different types of sintered alumina (at various densities and compositions) show Vickers hardness values of about 15 to 20 GPa. They estimate the actual microhardness values for some of the samples to be as high as 25 GPa, but porosity effects are believed to give lower values. These data are included in Table 82.VII.

Several other references, summarized in Table 82.VII, give bulk microhardness data for materials of interest. Okuyama *et al.*,[41] Nathan,[42] and Brecker *et al.*[43] give hardness data for alumina (Al_2O_3) and silicon carbide (SiC). These references suggest a Moh's hardness of about 9, and an approximate Knoop microhardness of 20±3 GPa for alumina and 27±5 GPa for SiC. Nassau[44] gives the hardness of cubic zirconia between 8.0 and 8.5 on the Moh's scale. Since alumina and SiC have a Moh's hardness of about 9, we can expect cubic zirconia to have a Knoop microhardness similar to, but slightly less than that of Al_2O_3 and SiC. There is, however, no direct relationship between the two hardness scales. No details about these microhardness measurements are given.

Some information on the hardness of cerium oxide is also available in the literature. Izumitani[4] states that cerium oxide has an approximate Moh's hardness of 6 and that most optical glasses range from 5 to 6 on the same hardness scale. Therefore we can expect the hardness of cerium oxide to be of the order of BK7 and FS glasses. While West[45] does not give a number for the hardness of cerium oxide, he does discuss how thermal treatments at elevated temperatures cause cerium oxide to become harder. Izumitani[4] also discusses the heat treatment of cerium oxide and confirms West's result. We will show a similar result with our experiments.

Table 82.VII: Summary of hardness data from the literature for various abrasive materials.

Abrasive	Mohs Hardness(Ref)	Knoop Hardness (Gpa)	Vickers Hardness (Gpa)
Alumina[a,c]	9(41), 9.4(42)	16.58–24.22(41,43)	–
Sintered alumina[b]	–	–	15–25(28)
Zirconia[c]	8.0–8.5(44)	–	–
Cerium oxide[c]	6(4)	–	–
Silicon carbide[a]	9.6(42)	22.15–31.63(41,43)	–

[a]Microhardness tests of bulk material

[b]Microhardness tests of large particles

[c]Moh's tests not well defined

Results

Tables 82.VIII to 82.X show the results from our experiments. Table 82.VIII gives the 11 magnetic particles that were tested with the nanoindenter: ten are carbonyl iron and one is a carbonyl nickel. The types and vendor plus information on the composition and nanohardness of each particle are listed. Table 82.IX lists the nonmagnetic abrasives along with their vendor, crystal structure, and nanohardness information. We also indented two optical glasses (BK7[13] and fused silica, FS[46]), one laser glass (LHG8[47]), and a soft crystal (potassium dihydrogen phosphate, KDP[48]) under identical conditions for comparison. Information on these materials is given in Table 82.X.

Figure 82.65 shows the relative nanohardness values for the different particles compared to the reference glasses. First, consider the CI particles: the hard CI's are as hard (S-1701) or harder (EW, OS 3770, OS 1225, OS 2983, OM) than fused silica. The soft, reduced forms of the CI's are significantly softer than all of the glasses and comparable in hardness to KDP. Two of the OS samples (OS 5942 and OS 9560) have intermediate nanohardness values due to a variation of processing parameters. Some of the nanohardness values measured for hard particles are harder than those cited in the literature, while others are in good agreement with the numbers cited. The soft CI's are much softer, as suggested by the literature. The nickel proved to be an extremely soft particle, in contradiction to our expectations from discussions with the manufacturer.

The differences in nanohardness among the hard CI samples can be analyzed further. The heat treatment process and the presence of impurities play a significant role in determining hardness of the particles. The reduction process softens the particles by removing the impurities in the iron. Conversely, it has been shown that the inclusion of some of these impurities often hardens iron (see, for example, Refs. 58 and 59). It is not known if the impurities are present in atomic or molecular form. It would be expected that impurities strengthen a metal as the square root or cube root of the concentration whether in atomic or molecular form.[60] Specifically, it is expected that the hardness of iron will increase as the square

Table 82.VIII: Summary of the manufacturer information and nanohardness results for the indented magnetic particles, given in rank order from hardest to softest.

ID	Material	Lot Number[Mfr.]	$b_{wt\%}$			Hardness by Nanoindentation (standard deviation) (Gpa)	
			Nitrogen	Carbon	Oxygen		
OS 1225	Carbonyl iron	1225[(49)]	[0.540	0.880	0.580][(52)]	14.4	(0.8)
OS 2983	Carbonyl iron	2983[(49)]	[0.750	0.800	0.590][(52)]	13.1	(0.6)
OM	Carbonyl iron	3999[(49)]	0.800	0.790	0.240	12.4	(1.0)
EW	Carbonyl iron	9970[(49)]	1.000	0.800	0.500	11.7	(0.8)
OS 3770	Carbonyl iron	3770[(49)]	[0.180	1.120	0.650][(52)]	10.5	(1.0)
S-1701	Carbonyl iron	6070111[(50)]	0.850	0.850	0.730	9.7	(0.5)
OS 5942	Carbonyl iron	5942[(49)]	0.060	1.170	0.320	7.3	(1.0)
OS 9560	Carbonyl iron	9560[(49)]	1.180	0.970	0.200	4.9	(1.0)
CM	[a]Carbonyl iron	7829[(49)]	[<0.010	0.009	0.170][(52)]	2.4	(0.5)
R-1521	[a]Carbonyl iron	8052131[(50)]	0.024	0.033	0.240	2.2	(1.0)
Nickel	Carbonyl nickel	101397[(51)]				1.7	(0.6)

[a]Reduced form of particle
[b]Amount of residual nitrogen, oxygen, and carbon in the carbonyl icons is in weight percent, usually per certificate of analysis from the manufacturer.

root or cube root of the concentration of carbon, nitrogen, and oxygen (in this order for the hardening effect).[61] Using the amounts of residual carbon and nitrogen provided by the vendor, nanohardness values are plotted as a function of the total amount of carbon and nitrogen in Fig. 82.66. The OS samples show a relatively large variation in nanohardness; therefore, data for all OS samples have been averaged into a single data point with error bars representing a standard deviation. After discussions with the company, we hypothesize that variations in their internal processing methods, such as annealing, were responsible for this variation in the nanohardness data. The data have been fit with a simple power law curve on a log-log scale, and the equation and correlation coefficient are shown with the plot. Notice that the data fit (correlation better than 0.94) a power law of about 0.38. While the variation due to the OS samples is somewhat large, this trend in the nanohardness as a function of impurity content is in the expected range.

The data for the polishing abrasives reveal some interesting features. The nanohardness values of the #30 grinding alumina, silicon carbide, cubic zirconia, and cerium oxide samples agree with microhardness and Moh's hardness values reported for bulk materials (compare Tables 82.VII and 82.IX), validating our results. The 1-μm alumina has a significantly lower nanohardness than the grinding alumina—a surprising result that can be attributed to proprietary manufacturing methods.[62]

We report for the first time on nanohardness data for cerium oxide abrasives. The two cerium oxides, SRS 372 and SRS 373, differed only in their heat treatments. Specifically, SRS 372 had a higher thermal treatment than did SRS 373.[63] This resulted in SRS 372 having about a 50% higher nanohardness than SRS 373, which agrees with descriptions of heat-treated cerium oxide given by Izumitani[4] and West.[45]

Table 82.IX: Summary of the manufacturer information and nanohardness results for the indented nonmagnetic abrasives, given in rank order from hardest to softest.

ID	Material	Lot Number[Mfr.]	Crystal Structure	Hardness by Nanoindentation (standard deviation) (Gpa)	
SiC	Silicon carbide	[a]N/A(53)	Hexagonal	31.8	(8.0)
#30 Al_2O_3	Grinding alumina	C9043(54)	Hexagonal	29.8	(7.0)
CZ	Cubic zirconia	1502792(55)	Cubic	24.1	(5.0)
1 μm Al_2O_3	Polishing alumina	C602(56)	Not reported	10.0	(4.0)
SRS 372[b]	Cerium oxide	SDH-13-1(57)	Not reported	7.5	(2.0)
SRS 373[c]	Cerium oxide	SDH-13-2(57)	Not reported	5.0	(1.3)

[a]Lot number is not available. Abrasives were received in 8/94.
[b]High thermal treatment
[c]Low thermal treatment

Table 82.X: Summary of the manufacturer information and nanohardness results for the indented bulk optical materials given in rank order from hardest to softest.

ID	Lot Number[Mfr.]	Hardness by Nanoindentation (standard deviation) (Gpa)	
FS	7940(46)	9.8	(0.1)
BK7	N/A(13)	7.7	(0.1)
LHG8	N/A(47)	5.3	(0.1)
KDP	N/A(48)	1.5	(0.4)

The error bars for the magnetic abrasives and optical materials are considerably smaller than those of the polishing abrasives. This is attributed to the more uniform structure of CI and the optical materials versus the multiphase nature and heterogeneity of the polishing abrasives tested. Krell *et al.*[28] also had relatively large errors in their measurements, which they attributed to microstructure. We do not have control of the crystal orientation of the abrasives that we are indenting, which will also affect the measured nanohardness.

Summary

A technique for nanoindentation of small, magnetic and nonmagnetic abrasive particles has been described. Most results are consistent with what has been previously reported, but some results are new. While Krell *et al.*[28] show microhardness differences in various grinding aluminas, it is interesting to see the large differences in nanohardness values of the actual commercial products used in grinding and polishing.

The literature contains only Moh's hardness data for cerium oxide abrasives. We report here, for the first time, an actual nanohardness value for individual cerium oxide abrasives. The tests and procedures described here allow for the characterization of the mechanical properties of small particles that is not possible through microindentation without sintering or using samples much larger than those normally used. This allows for the study of abrasives in forms actually used in polishing, so that full characterization of the mechanical properties of polishing materials is now possible. Furthermore, removal experiments using various combinations of magnetic and nonmagnetic abrasive particles and slurry fluid chemistries should give valuable information in the future regarding the removal mechanisms for MRF.

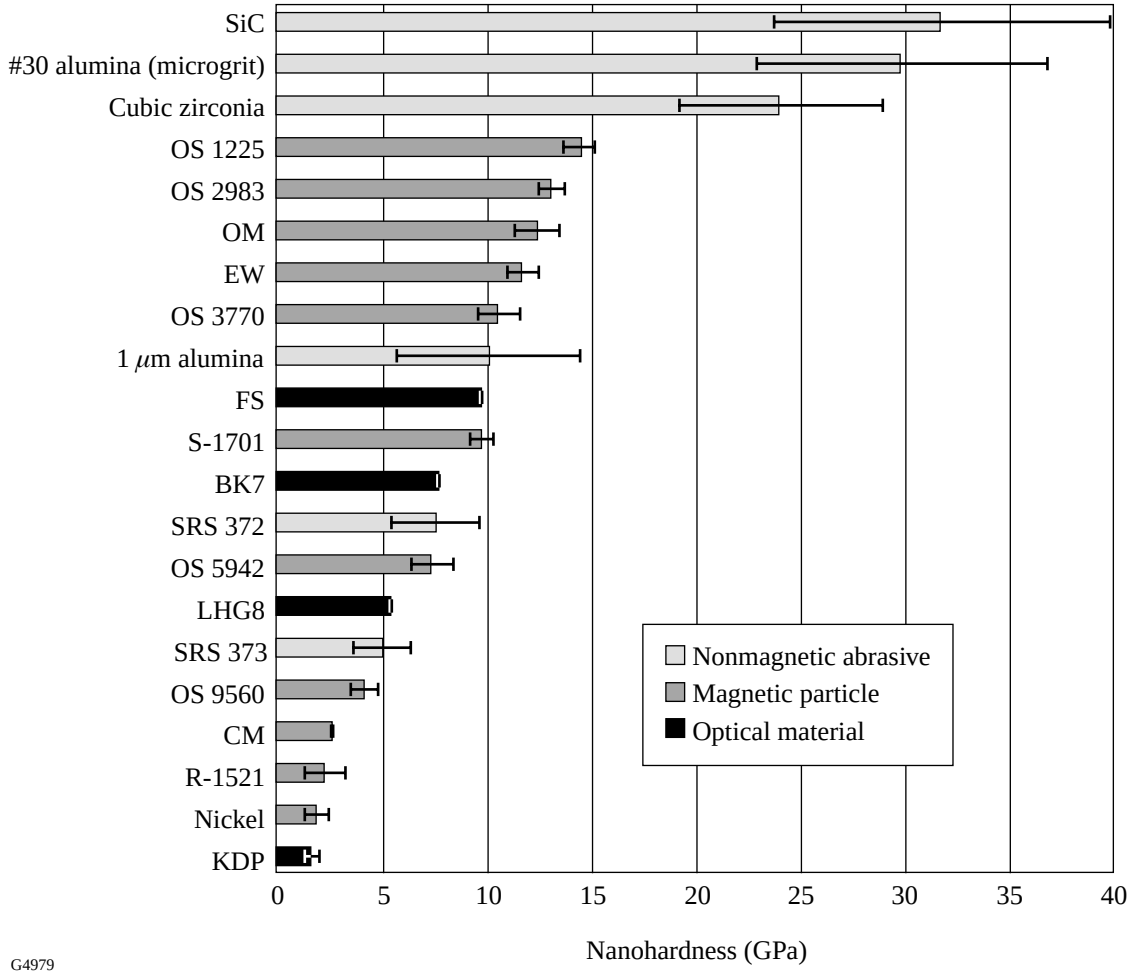

Figure 82.65
The relative nanohardness values of the particles, glasses, and crystal that have been indented (in air) at 5-mN load on the nanoindenter.

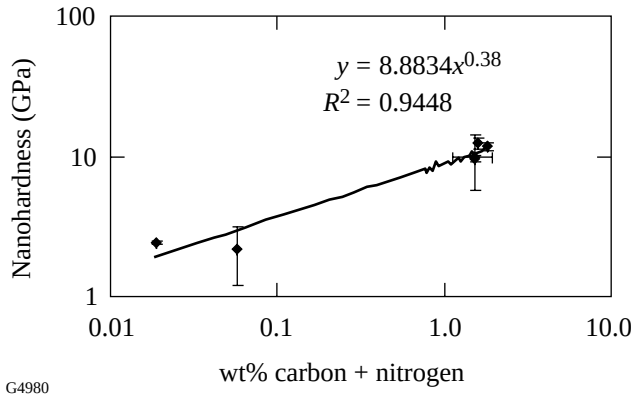

Figure 82.66
Particle nanohardness as a function of the sum of carbon and nitrogen present. An expected power law dependence is seen. Similar results are achieved if only nitrogen or carbon is analyzed.

ACKNOWLEDGMENT

The authors would like to thank Professor John C. Lambropoulos of the Mechanical Engineering Department of the University of Rochester for his assistance. We also acknowledge the contributions of Cindy Barnett and Becky Coppens of the COM and Gail Schlosser and Lisa Cliff of LLE for assistance in preparation of this article; Alexander Maltsev of the LLE and Dennis Van Gee of the COM for assistance in sample preparation, Professor Roger Gans of the Mechanical Engineering Department, Professor James Li of the Materials Science Program at the University of Rochester and Bob Nesin of Micro Abrasives for helpful discussions. Brian McIntyre of the Optics Department at the University of Rochester is acknowledged for his work on the SEM. We would also like to thank Jennifer Murphy, Susan Brandt, Rosa Lee, Caleb Farny, Leslie Gregg, and Dr. Steven Arrasmith for their participation in the project. Dr. Al Friederang of BASF Corporation and Ms. Dana Zagari of Ferro Corporation are thanked for providing many different samples. Support for this work was provided in part by a Department of Education graduate fellowship (GAANN), QED Technologies, LLC, Byelocorp Scientific, Inc, U.S. Army Materiel Command, DARPA (Defense Advanced Research Project Agency), and the National Science Foundation (Grant CMS-9601585).

REFERENCES

1. D. Golini, S. Jacobs, W. Kordonski, and P. Dumas, in *Advanced Materials for Optics and Precision Structures*, edited by M. A. Ealey, R. A. Paquin, and T. B. Parsonage, Critical Reviews of Optical Science and Technology (SPIE, Bellingham, WA, 1997), Vol. CR67, pp. 251–274.

2. Zygo New View™ 100 White-Light Interferometer, 20× Mirau objective, Zygo Corporation, Middlefield, CT 06455.

3. S. D. Jacobs, W. Kordonski, I. V. Prokhorov, D. Golini, G. R. Gorodkin, and T. D. Strafford, U.S. Patent No. 5,795,212 (18 August 1998).

4. T. S. Izumitani, *Optical Glass*, American Institute of Physics Translation Series (American Institute of Physics, New York, 1986), pp. 92–98.

5. A. Kaller, Glass Sci. Technol. **71**, 174 (1998).

6. A. B. Shorey, L. L. Gregg, H. J. Romanofsky, S. R. Arrasmith, I. Kozhinova, J. Hubregsen, and S. D. Jacobs, in *Optical Manufacturing and Testing III*, edited by H. Stahl (SPIE, Bellingham, WA, 1999), Vol. 3782, pp. 101–111.

7. R. Steinitz, Metals & Alloys **17**, 1183 (1943).

8. Nano IIs Nanoindentor and accompanying operating instructions, Version 2.2, p. 7 (1996), Nano Instruments, Oak Ridge, TN 37830.

9. W. C. Oliver and G. M. Pharr, J. Mater. Res. **7**, 1564 (1992).

10. G. M. Pharr and W. C. Oliver, Mater. Res. Bull. **17**, 28 (1992).

11. J. C. Hay and G. M. Pharr, in *Thin-Films—Stresses and Mechanical Properties VII*, edited by R. C. Cammarata *et al.*, Mat. Res. Soc. Symp. Proc. Vol. 505 (Materials Research Society, Warrendale, PA, 1998), pp. 65–70.

12. 16- to 18-μm wire mesh sieve, Newark Wire Cloth Company, Newark, NJ 07104.

13. 2.54 × 1.27 × 0.64-cm samples made from material provided by Schott Glass Technologies, Duryea, PA 18642.

14. Samarium-Cobalt magnets (2.54 × 2.54 × 1.08 cm) purchased from the McMaster-Carr Supply Company, Elmhurst, IL 60126. They supply a field intensity of about 2.5 kG in a direction perpendicular to the surface of the magnet.

15. 2-Ton® Clear Epoxy from ITW Devcon, Danvers, MA 01923.

16. Kapton® is a polyamide film provided by DuPont®. We used type HV300. Teflon® films have also been used.

17. Y. Grasselli, G. Bossis, and E. Lemaire, Prog. Colloid Polym. Sci. **93**, 175 (1993).

18. Microgrit Micro Abrasives Corporation, Westfield, MA 01086-0669.

19. R. E. Parks, R. E. Sumner, and J. T. Appels, Opt. Eng. **16**, 332 (1977).

20. Load was measured by the I-Scan pressure measurement system from Tekscan, Inc., Boston, MA 02127. We used a 5051 pressure film with a maximum allowable load of 345 kPa (50 psi).

21. J. H. Rhodes, # FJ0202, Universal Photonics, Inc., Hicksville, NY 11801-1014.

22. Olympus VANOX-T AH-2 optical microscope, No. 501008, Olympus Optical Co. Ltd., Tokyo, Japan.

23. Measurements were made using the Form Talysurf® mechanical profilometer, Taylor Hobson Ltd., Leicester, LE4 9JQ, UK. The device has a 60-mm stylus arm length and a 2-μm-radius tip.

24. Buehler Ltd., Lake Bluff, IL 60044-1699.

25. LEO 982 field emission SEM (LEO is a Zeiss-Leica company).

26. *Metals Test Methods and Analytical Procedures*, Annual Book of ASTM Standards (American Society for Testing and Materials, West Conshohocken, PA, 1999), Vol. 3.01, p. 393.

27. I. N. Sneddon, *Fourier Transforms*, 1st ed. (McGraw-Hill, New York, 1951), Sec. 52.5.

28. A. Krell, P. Blank, E. Wagner, and G. Bartels, J. Am. Ceram. Soc. **79**, 763 (1996).

29. J. C. Lambropoulos, T. Fang, P. D. Funkenbusch, S. D. Jacobs, M. J. Cumbo, and D. Golini, Appl. Opt. **35**, 4448 (1996).

30. T. Fang, "Near-Surface Mechanical Properties of Optical Materials in Deterministic Microgrinding," Ph.D. thesis, University of Rochester, 1997, Chap. 3.

31. K. Sangwal *et al.*, J. Mater. Res. **14**, 3973 (1999).

32. F. Dahmani, J. C. Lambropoulos, A. W. Schmid, S. J. Burns, and C. Pratt, J. Mater. Sci. **33**, 4677 (1998).

33. J. H. Westbrook, Phys. Chem. Glasses **1**, 32 (1960).

34. D. Tabor, Proc. Phys. Soc., Sec. B **67**, 249 (1954).

35. W. D. Callister, *Materials Science and Engineering*, 2nd ed. (Wiley, New York, 1991), pp. 131-141.

36. S. Ramarajan *et al.*, Surf. Eng. **15**, 324 (1999).

37. L. B. Pfeil, *Symposium on Powder Metallurgy*, 47, The Iron and Steel Institute, Grosvenor Gardens, London, Special Report No. 38 (1947).

38. F. L. Ebenhoech, Prog. Powder Metall. **42**, 133 (1986).

39. J. E. Japka, J. Met. **40**, 18 (1988).

40. G. Boehm, Fachber. Huettenprax. Metallweiterverarb. **20**, 146 (1982).

41. K. Okuyama and Y. Kousaka, in *Powder Technology Handbook*, edited by K. Iinoya, K. Gotoh, and K. Higashitani (Marcel Dekker, New York, 1991), pp. 57–61.

42. G. K. Nathan and W. J. D. Jones, Proc. Instn. Mech. Engrs. **181**, 215 (1966–67).

43. J. N. Brecker, R. Komanduri, and M. C. Shaw, Ann. CIRP **22**, 219 (1973).

44. K. Nassau, Lapidary J. **35**, 1194 (1981).

45. C. A. West, Can. Chem. Process Inds. **28**, 3 (1944).

46. Corning 7940, Corning, Inc., Corning, NY 14831-0002.

47. LHG8, Hoya Corporation USA, San Jose, CA 95131.

48. KDP provided by Cleveland Crystals, Inc. (CCI), Cleveland, OH 44110. Indents were done on a fractured surface (Type-II cut).

49. BASF Corporation, Mt. Olive, NJ 07828-1234.

50. ISP International, Wayne, NJ 07470.

51. Novamet, Wyckoff, NJ 07481.

52. Personal communication with Dr. Al Friederang, BASF Corporation, 28 July 1998.

53. Exolon-Esk Company, Tonawanda, NY 14151-0590.

54. Microabrasives Corporation, Westfield, MA 01085.

55. Zirconia I, batch #1502792, courtesy of Saint Gobain/Norton Industrial Ceramics Corporation, Worcester, MA 15136.

56. 1.0-μm C, alumina polishing compound, Praxair Surface Technologies, Indianapolis, IN 46222-3274.

57. Transelco Division of Ferro Corporation, Penn Yan, NY 14527.

58. C. R. Brooks, *Heat Treatment of Ferrous Alloys* (Hemisphere, Washington, 1979).

59. T. Fujihana *et al.*, Surf. Coat. Technol. **51**, 19 (1992).

60. J. D. Verhoeven, *Fundamentals of Physical Metallurgy* (Wiley, New York, 1975), Chaps. 11 and 14.

61. Personal communication with Prof. James C. Li, Materials Science Program, University of Rochester, 1998.

62. Personal communication with Dr. James Knapp, Praxair Surface Technologies, 1999.

63. Personal communication with Ms. Dana Zagari, Transelco Division of Ferro Corporation, 1999.